Molecular Therapy
Oncolytics
Original Article

DNA-methylation-induced silencing of DIO3OS drives non-small cell lung cancer progression via activating hnRNPK-MYC-CDC25A axis

Meichun Zhang,[1] Jing Wu,[2] Weinong Zhong,[1] Ziwen Zhao,[1] and Weiguo He[1]

[1]Department of Pulmonary and Critical Care Medicine, Guangzhou First People's Hospital, School of Medicine, South China University of Technology, No. 1 Panfu Road, Guangzhou 510180, China; [2]Department of Central Sterile Supply, Guangzhou First People's Hospital, School of Medicine, South China University of Technology, Guangzhou 510180, China

DNA methylation is a class of epigenetic modification manner, which is responsible for the inactivation of various tumor suppressors. Recently, long non-coding RNAs (lncRNAs) were revealed to be implicated in a variety of malignancies, including non-small cell lung cancer (NSCLC). However, the contributions of lncRNAs to DNA-methylation-induced oncogenic effects in NSCLC remain largely unknown. In this study, we identified a DNA-methylation-repressed lncRNA DIO3 opposite strand upstream RNA (DIO3OS) in NSCLC. DIO3OS is downregulated in NSCLC, and its low expression is related to poor prognosis. Ectopic expression of DIO3OS repressed NSCLC cell growth and motility and promoted NSCLC cell apoptosis *in vitro*. DIO3OS also repressed NSCLC tumorigenesis and metastasis *in vivo*. DIO3OS knockdown exhibited opposite biological effects. DIO3OS competitively bound heterogeneous nuclear ribonucleoprotein K (hnRNPK), repressed the binding of hnRNPK to *MYC* DNA and MYC mRNA, reduced the promoting roles of hnRNPK on *MYC* transcription and translation, led to the repression of *MYC* transcription and translation, and therefore remarkably decreased the expression of MYC and CDC25A, a downstream target of MYC. Additionally, depletion of hnRNPK blocked the tumor-suppressive roles of DIO3OS in NSCLC. In conclusion, these findings identified DIO3OS as an important protective factor against NSCLC via modulating hnRNPK-MYC-CDC25A axis.

INTRODUCTION

Lung cancer is the second most common malignancy and primary cause of cancer-related death according to global cancer statistics 2020.[1] 2,206,771 new lung cancer cases and 1,796,144 lung-cancer-related deaths were estimated to occur in 2020 worldwide, accounting for 11.4% of the total new cancer cases and 18.0% of the total new cancer deaths.[2] Pathologically, lung cancer is classified into small cell lung cancer (SCLC), lung adenocarcinoma (LUAD), lung squamous cell carcinoma (LUSC), and large cell lung cancer. LUAD, LUSC, and large cell lung cancer were also classed as non-small cell lung cancer (NSCLC), which constitutes more than 85% of all lung cancer cases.[3] Although regional early NSCLC could be cured by surgical resection, the prognosis of most unresectable NSCLC patients is still unfavorable, with 5-year survival rate of less than 10%.[4] Therefore, there is a critical need to reveal the underlying molecular mechanisms in NSCLC and develop more effective therapeutic strategy against NSCLC.

Increasing evidences in gene expression profiles of NSCLC have identified many aberrantly expressed genes, such as the upregulation of oncogenes and downregulation of tumor suppressors.[5] Epigenetic factors exhibit pivotal roles in the modulation of genes expression.[6] Aberrant epigenetic modifications may promote NSCLC progression via regulating the expression of oncogenes or tumor suppressors.[7] DNA methylation is one important type of epigenetic modifications, which silences target genes expression.[8] Several protein-encoding genes have been identified as targets regulated by DNA methylation, such as *ALDH2*, *LMX1A*, and *SLC22A18*.[9–11] The hypermethylation or hypomethylation causes downregulation or overexpression of target genes, which further regulate NSCLC tumorigenesis and progression.[12]

Apart from protein-encoding genes, several non-coding RNAs were also identified to be targets of DNA methylation, such as miR-21 and miR-196b.[12,13] The aberrant expressions and functions of microRNAs (miRNAs) have been reported in various malignancies, including NSCLC.[14–16] Recent transcriptomic sequencings have identified more than 58,000 long non-coding RNAs (lncRNAs).[17] lncRNAs is a class of transcripts with more than 200 nt in length and limited protein-coding ability.[18] Many lncRNAs were also found to be aberrantly expressed in various diseases.[19–25] Additionally, lncRNAs also exhibit pivotal roles in a variety of pathophysiological processes.[26–33] Several lncRNAs were revealed to play oncogenic or tumor-suppressive roles in NSCLC, such as the oncogenic lncRNA LINC01561, SNHG15, and LINC00173.v1, and the tumor-suppressive lncRNA CASC7, BRCAT54, and NORAD.[34–39] However, the

Received 6 April 2021; accepted 24 September 2021;
https://doi.org/10.1016/j.omto.2021.09.006.

Correspondence: Dr. Meichun Zhang, Department of Pulmonary and Critical Care Medicine, Guangzhou First People's Hospital, School of Medicine, South China University of Technology, No. 1 Panfu Road, Guangzhou 510180, China.
E-mail: drzhangmc@sina.com

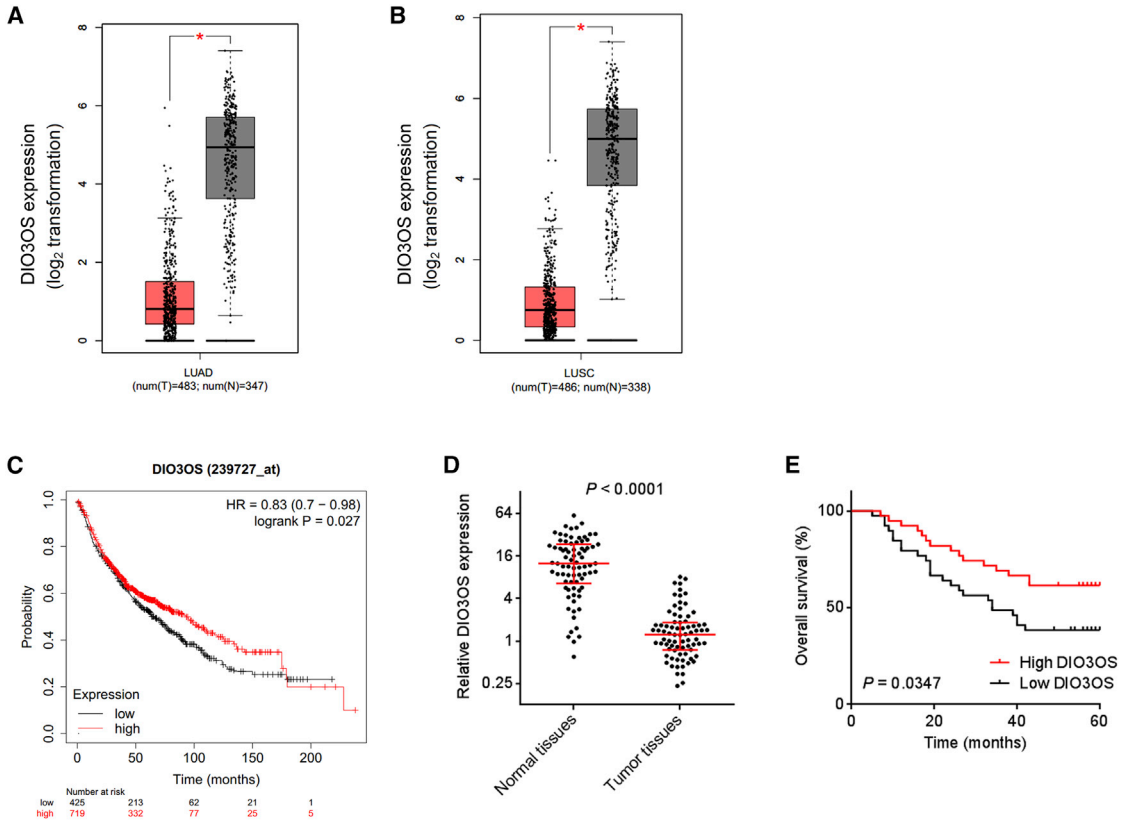

Figure 1. DIO3OS was downregulated, and its low expression was related with poor prognosis in NSCLC

(A) DIO3OS expression in LUAD tissues (T) and normal tissues (N) from TCGA dataset analyzed by GEPIA. (B) DIO3OS expression in LUSC tissues (T) and normal tissues (N) from TCGA dataset analyzed by GEPIA is shown. (C) The correlation between DIO3OS expression and overall survival in NSCLC analyzed by Kaplan-Meier Plotter is shown. (D) DIO3OS expression levels in 78 pairs of NSCLC tissues and matched adjacent normal lung tissues were measured by quantitative real-time PCR. Data are shown as median with interquartile range. $p < 0.0001$ by Wilcoxon matched-pairs signed rank test. (E) Kaplan-Meier analysis of the correlation between DIO3OS expression and overall survival of these 78 NSCLC patients is shown. $p = 0.0347$ by log rank test.

factors contributing to the dysregulation of lncRNAs in NSCLC remain largely unresolved. Furthermore, whether DNA methylation modulates lncRNA expression in NSCLC needs further investigation.

In this study, through analyzing The Cancer Genome Atlas (TCGA) dataset, we identified a DNA-methylation-modulated lncRNA DIO3 opposite strand upstream RNA (DIO3OS). We found that DIO3OS was significantly downregulated in NSCLC, and its low expression was related to poor prognosis. Gain- and loss-of-function approaches revealed that DIO3OS significantly repressed NSCLC cell growth and mobility and promoted NSCLC cell apoptosis *in vitro* and also repressed NSCLC tumorigenesis and metastasis *in vivo*. The underlying molecular mechanisms mediating the roles of DIO3OS in NSCLC were investigated.

RESULTS

DIO3OS is downregulated in NSCLC, and its low expression is related to disease progress and poor prognosis

To search the lncRNAs differently expressed in NSCLC, we analyzed TCGA dataset using the online tool Gene Expression Profiling Interactive Analysis (GEPIA) (http://gepia.cancer-pku.cn/). The 100 most significantly downregulated lncRNAs were shown in Table S1. Among these lncRNAs, we noted DIO3OS, which was not only significantly downregulated in LUAD (Figure 1A) but also significantly downregulated in LUSC (Figure 1B). Additionally, TCGA dataset also revealed that low expression of DIO3OS was related to shorter overall survival (Figure 1C), analyzed by Kaplan-Meier Plotter (http://kmplot.com/analysis/). To further validate the clinical relevance of DIO3OS in NSCLC, we collected 78 pairs of NSCLC tissues and matched adjacent normal lung tissues. Quantitative real-time polymerase chain reaction (PCR) results showed that DIO3OS was remarkably downregulated in NSCLC tissues compared to normal tissues (Figure 1D). Correlation analyses of DIO3OS expression and clinicopathological features revealed that low expression of DIO3OS was related to local invasion, lymphatic metastasis, and advanced Tumor, Node, Metastasis (TNM) stage (Table 1). Kaplan-Meier analysis revealed that low expression of DIO3OS was related to worse overall survival (Figure 1E). Thus, these data collectively demonstrated that DIO3OS was downregulated in NSCLC, and its low expression was related to disease progress and poor prognosis.

Table 1. Relationships between DIO3OS expression and clinicopathological features in NSCLC

Parameter	No. of patients	DIO3OS		p value
		Low	High	
Age				0.642
≥60	48	25	23	
<60	30	14	16	
Gender				0.482
Male	49	26	23	
Female	29	13	16	
Histologic				0.255
Squamous carcinoma	43	24	19	
Adenocarcinoma	35	15	20	
Tumor size				0.113
≤3 cm	39	16	23	
>3 cm	39	23	16	
Local invasion				0.044
T1+T2	63	28	35	
T3+T4	15	11	4	
Lymphatic metastasis				0.037
Negative	47	19	28	
Positive	31	20	11	
TNM stage				0.015
I	33	12	21	
II	24	11	13	
III	21	16	5	

p values were calculated by Pearson chi square test.

CpG456 methylation downregulates DIO3OS expression

Epigenetic alterations in promoter region play pivotal roles in the aberrant expression of genes.[19] Intriguingly, the *DIO3OS* promoter is located on a CpG island, CpG456 (Figure 2A). Thus, we next determined whether low expression of DIO3OS is correlated with methylation of CpG456. Seventeen methylation probes located on *DIO3OS* promoter and CpG456 with methylation data were retrieved from TCGA Illumina Infinium Human DNA Methylation 450k BeadChip data using the online tool UCSC Xena (https://xenabrowser.net/heatmap/#). Then, the correlation between DIO3OS expression and CpG456 methylation status in TCGA NSCLC samples was calculated. Pearson correlation analyses revealed that all 17 methylation probes in CpG456 were remarkably inversely correlated with DIO3OS expression in NSCLC (Figures 2B–2D and S1). Moreover, the DNA methylation levels of *DIO3OS* promoter were detected using bisulfate sequencing in NSCLC tissues and matched adjacent normal lung tissues. The results revealed that DNA methylation levels of *DIO3OS* promoter were much higher in NSCLC tissues compared with those in normal lung tissues (Figure 2E). Treatment of NSCLC cells with the demethylation reagent 5-Aza remarkably increased DIO3OS expression (Figures 2F and 2G). Therefore, the data suggested that methylation at *DIO3OS* promoter-associated CpG456 at least partially contributed to the low expression of DIO3OS in NSCLC.

DIO3OS represses NSCLC cell growth and motility and promotes NSCLC cell apoptosis *in vitro*

To explore the potential biological effects of DIO3OS in NSCLC, H1299 and H1975 cells with DIO3OS stable overexpression were constructed through transfection of DIO3OS overexpression vector. The overexpression efficiencies were confirmed by quantitative real-time PCR (Figures 3A and 3B). Cell Counting Kit-8 (CCK-8) assays revealed that cell growth of H1299 and H1975 cells was remarkably reduced after overexpression of DIO3OS (Figures 3C and 3D). Ethynyl deoxyuridine (EdU) incorporation assays validated that DIO3OS overexpressed H1299 and H1975 cells had less EdU-positive cells compared to control cells (Figures 3E and 3F), suggesting that overexpression of DIO3OS repressed NSCLC cell growth. To detect the effects of DIO3OS on NSCLC cell apoptosis, the activities of caspase-3 in cell lysates of H1299 and H1975 cells with DIO3OS stable overexpression were detected. The results revealed that caspase-3 activities were increased after DIO3OS overexpression in both H1299 and H1975 cells (Figures 3G and 3H), suggesting that DIO3OS overexpression promoted NSCLC cell apoptosis. To evaluate the effects of DIO3OS on NSCLC cell motility, transwell migration and invasion assays were conducted. Transwell migration assays revealed that cell migration abilities of H1299 and H1975 cells were both reduced after DIO3OS overexpression (Figures 3I and 3J). Transwell invasion assays revealed that cell invasion abilities of H1299 and H1975 cells were also both reduced after DIO3OS overexpression (Figures 3K and 3L). Taken together, these findings demonstrated that DIO3OS repressed NSCLC cell growth and motility and promoted NSCLC cell apoptosis *in vitro*.

Silencing DIO3OS promotes NSCLC cell growth and motility and represses NSCLC cell apoptosis *in vitro*

Apart from the effects of DIO3OS overexpression on NSCLC, we further investigated the effects of DIO3OS knockdown on NSCLC. A549 cells with DIO3OS stable knockdown were constructed through infection of two independent DIO3OS short hairpin RNA (shRNA) lentiviruses. The knockdown efficiencies were confirmed by quantitative real-time PCR (Figure 4A). CCK-8 assays revealed that cell growth of A549 cells was remarkably increased after DIO3OS knockdown (Figure 4B). EdU incorporation assays validated that DIO3OS-silenced A549 cells had significantly more EdU-positive cells compared to control cells (Figure 4C), suggesting that silencing DIO3OS promoted NSCLC cell growth. Caspase-3 activities in cell lysates of DIO3OS-silenced A549 cells were remarkably reduced compared to those in cell lysates of control A549 cells (Figure 4D), suggesting that silencing DIO3OS repressed NSCLC cell apoptosis. Transwell migration assays revealed that cell migration abilities of A549 cells were increased after DIO3OS silencing (Figure 4E). Transwell invasion assays revealed that cell-invasion abilities of A549 cells were also increased after DIO3OS silencing (Figure 4F). Taken together, these findings demonstrated that silencing DIO3OS promoted NSCLC cell growth and motility and

A

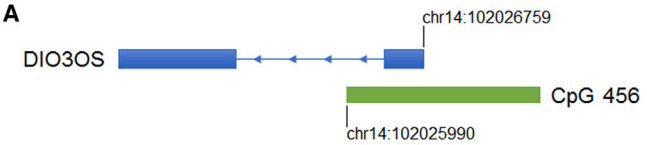

B

Methylation Probes (CpG 456) (chr:position)	DIO3OS	
	Pearson correlation coefficients	*P*-value
cg13126530 (chr14:102026230)	-0.3641	< 0.0001
cg02609127 (chr14:102026258)	-0.3570	< 0.0001
cg20560169 (chr14: 102026283)	-0.3789	< 0.0001
cg04818710 (chr14: 102026294)	-0.3234	< 0.0001
cg07193553 (chr14: 102026315)	-0.3444	< 0.0001
cg04623955 (chr14: 102026376)	-0.4239	< 0.0001
cg23354716 (chr14: 102026394)	-0.3366	< 0.0001
cg01044961 (chr14: 102026525)	-0.3049	< 0.0001
cg16781205 (chr14: 102026543)	-0.3386	< 0.0001
cg21174533 (chr14: 102026555)	-0.3412	< 0.0001
cg00328051 (chr14: 102026812)	-0.3438	< 0.0001
cg01693026 (chr14: 102026953)	-0.3852	< 0.0001
cg15238382 (chr14: 102027514)	-0.2987	< 0.0001
cg01664864 (chr14: 102027677)	-0.2665	< 0.0001
cg15341124 (chr14: 102027734)	-0.3106	< 0.0001
cg18804615 (chr14: 102027760)	-0.1904	0.0010
cg00741900 (chr14: 102027797)	-0.2815	< 0.0001

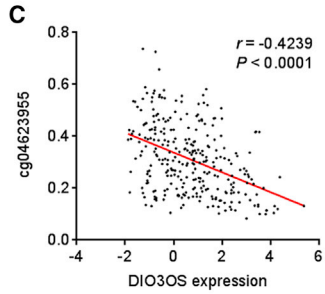

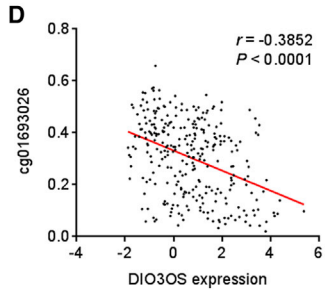

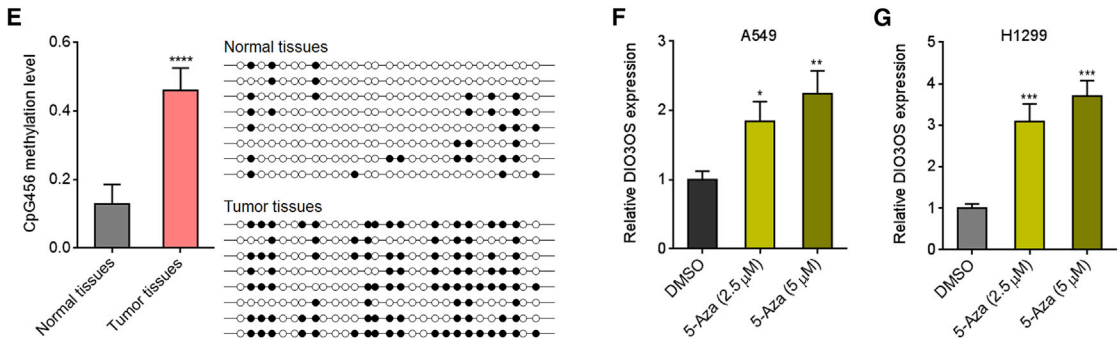

Figure 2. CpG456 methylation downregulated DIO3OS expression

(A) Schematic structure of *DIO3OS* genomic locus. (B) Correlation between DIO3OS expression from TCGA dataset and methylation probes in the promoter region of *DIO3OS* (CpG456) from TCGA Illumina Infinium Human DNA Methylation 450k BeadChip in NSCLC is shown. (C) Representative figure of correlation between DIO3OS expression and methylation probe cg04623955 (chr14: 102026376) in NSCLC is shown. (D) Representative figure of correlation between DIO3OS expression and methylation probe cg01693026 (chr14: 102026953) in NSCLC is shown. (E) Bisulfate DNA sequencing of *DIO3OS* promoter (CpG456) from 5 pairs of NSCLC tissues and normal lung tissues is shown. Data are shown as mean ± SD. ****$p < 0.0001$ by Student's t test. (F) DIO3OS expression in A549 cells after treatment with 2.5 μM or 5 μM 5-Aza for 3 days was detected by quantitative real-time PCR. (G) DIO3OS expression in H1299 cells after treatment with 2.5 μM or 5 μM 5-Aza for 3 days was detected by quantitative real-time PCR. For (F) and (G), data are shown as mean ± SD as determined by triple assays. *$p < 0.05$, **$p < 0.01$, and ***$p < 0.001$ by one-way ANOVA, followed by Dunnett's multiple comparisons test.

repressed NSCLC cell apoptosis *in vitro*. These gain- and loss-of-function experiments suggested that DIO3OS exhibits tumor suppressive roles *in vitro*.

DIO3OS represses NSCLC tumorigenesis and metastasis *in vivo*

To further validate the potential roles of DIO3OS in NSCLC tumorigenesis and metastasis *in vivo*, luciferase-labeled H1299 cells with DIO3OS stable overexpression or control were injected into tail vein of nude mice. 7 weeks after injection, bioluminescence analysis revealed that the mice injected with DIO3OS-overexpressed H1299 cells exhibited less lung tumorigenesis and metastases compared to those injected with control H1299 cells (Figure 5A). Histological analysis of lungs revealed that DIO3OS-overexpressed H1299 cells formed a smaller number of lung metastatic nodules and smaller nodular diameter compared to control H1299 cells (Figures 5B–5D). Additionally, luciferase-labeled A549 cells with DIO3OS stable knockdown or control were also injected into tail vein of nude mice. 7 weeks after injection, bioluminescence analysis revealed that

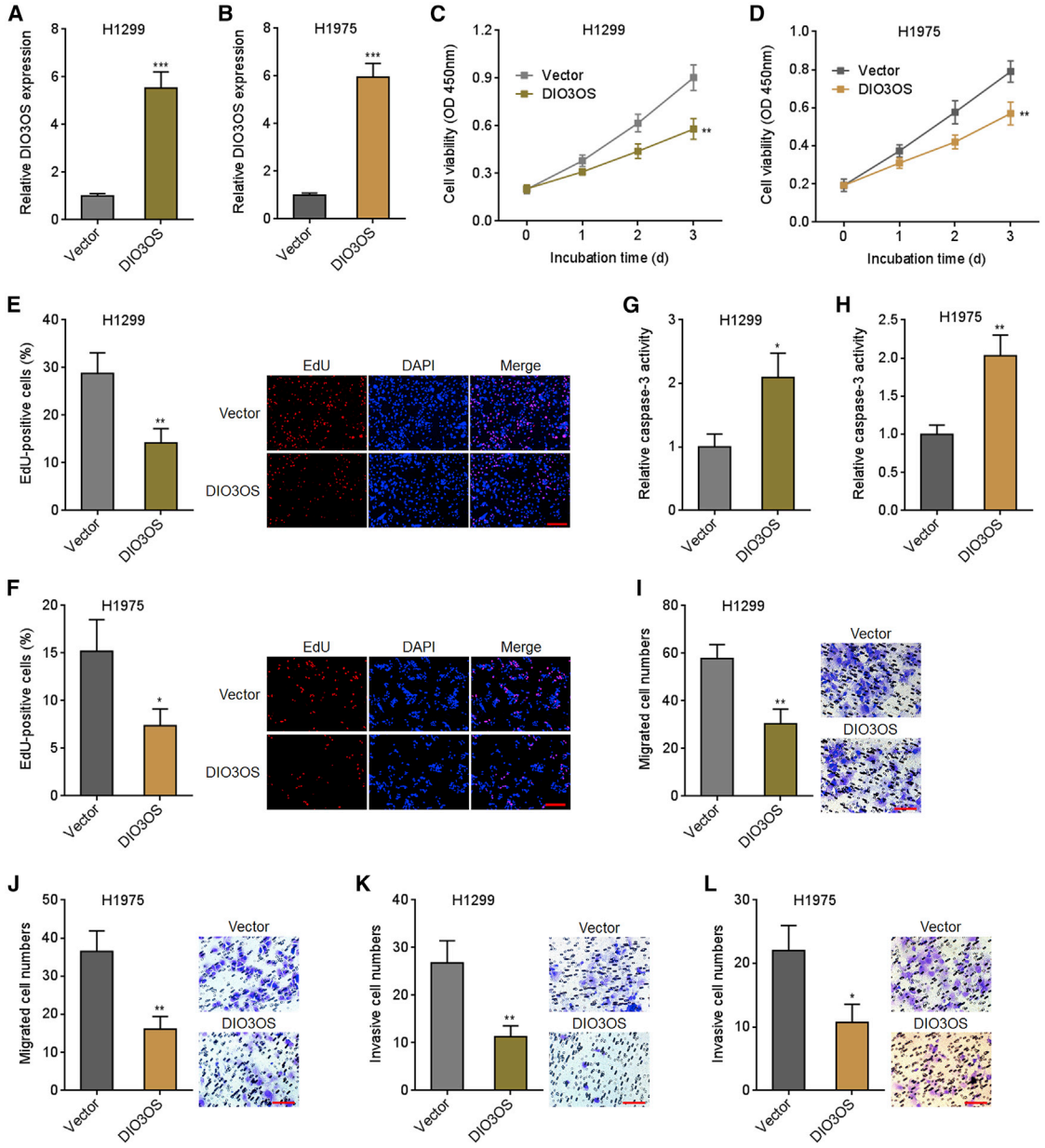

Figure 3. Ectopic expression of DIO3OS repressed NSCLC cell growth and mobility and promoted NSCLC cell apoptosis

(A) DIO3OS expression levels in H1299 cells with DIO3OS stable overexpression or control were measured by quantitative real-time PCR. (B) DIO3OS expression levels in H1975 cells with DIO3OS stable overexpression or control were measured by quantitative real-time PCR. (C) Cell growth of H1299 cells with DIO3OS overexpression or control was measured by CCK-8 assays. (D) Cell growth of H1975 cells with DIO3OS overexpression or control was measured by CCK-8 assays. (E) Cell growth of H1299 cells with DIO3OS overexpression or control was measured by EdU incorporation assays. Scale bars, 200 μm. (F) Cell growth of H1975 cells with DIO3OS overexpression or control were measured by EdU incorporation assays. Scale bars, 200 μm. (G) The activities of caspase-3 in cell lysates of H1299 cells with DIO3OS overexpression or control were measured to indicate cell apoptosis. (H) The activities of caspase-3 in cell lysates of H1975 cells with DIO3OS overexpression or control were measured to indicate cell apoptosis. (I) Cell migration of H1299 cells with DIO3OS overexpression or control was measured by transwell migration assays. Scale bars, 100 μm. (J) Cell migration of H1975 cells with DIO3OS overexpression or control was measured by transwell migration assays. Scale bars, 100 μm. (K) Cell invasion of H1299 cells with DIO3OS overexpression or control was measured by transwell invasion assays. Scale bars, 100 μm. (L) Cell invasion of H1975 cells with DIO3OS overexpression or control was measured by transwell invasion assays. Scale bars, 100 μm. Data are shown as mean ± SD as determined by triple assays. *$p < 0.05$, **$p < 0.01$, and ***$p < 0.001$ by Student's t test.

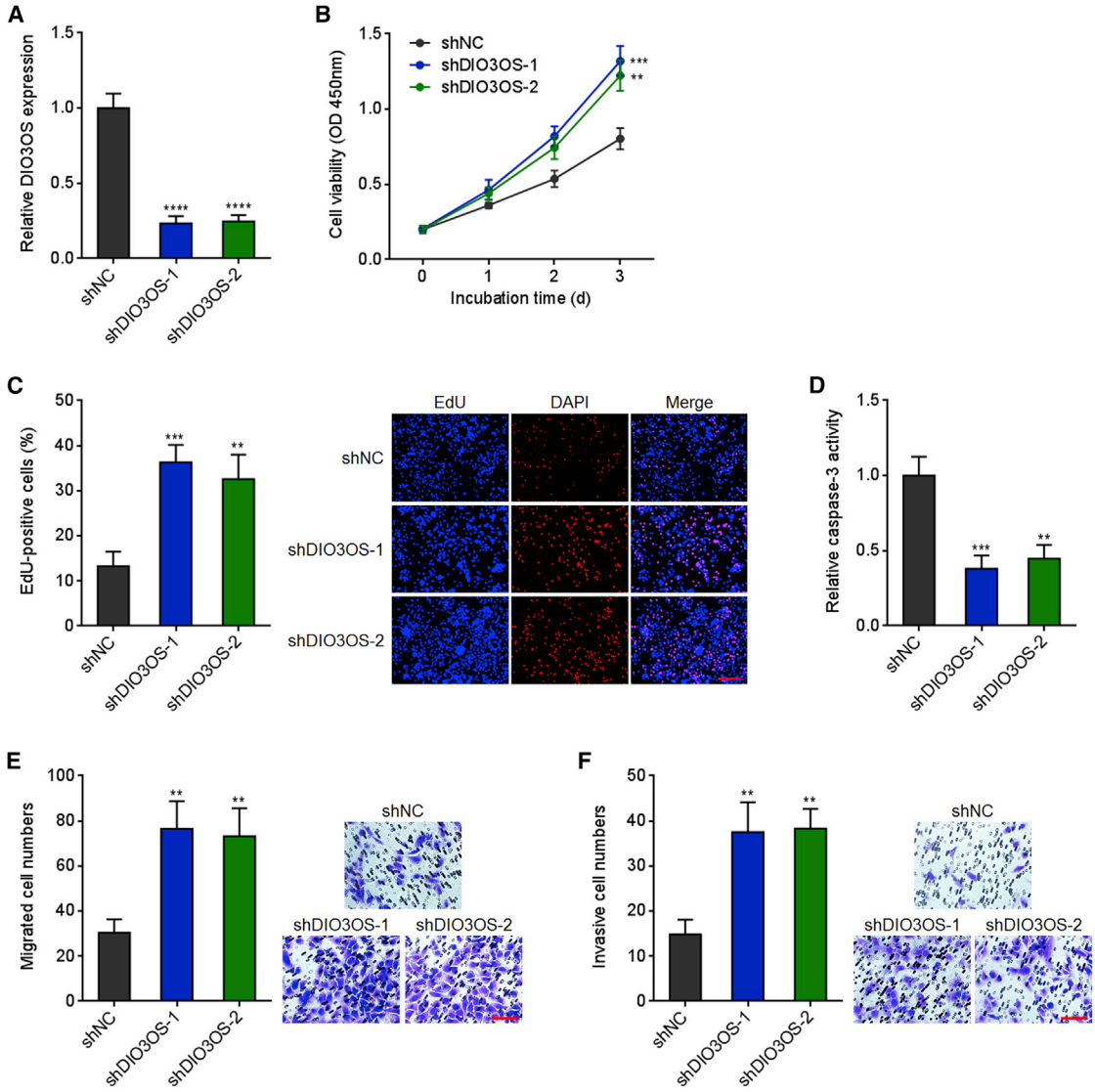

Figure 4. Depletion of DIO3OS promoted NSCLC cell growth and mobility and repressed NSCLC cell apoptosis

(A) DIO3OS expression levels in A549 cells with DIO3OS stable knockdown or control were measured by quantitative real-time PCR. (B) Cell growth of A549 cells with DIO3OS knockdown or control was measured by CCK-8 assays. (C) Cell growth of A549 cells with DIO3OS knockdown or control was measured by EdU incorporation assays. Scale bars, 200 μm. (D) The activities of caspase-3 in cell lysates of A549 cells with DIO3OS knockdown or control were measured to indicate cell apoptosis. (E) Cell migration of A549 cells with DIO3OS knockdown or control was measured by transwell migration assays. Scale bars, 100 μm. (F) Cell invasion of A549 cells with DIO3OS knockdown or control was measured by transwell invasion assays. Scale bars, 100 μm. Data are shown as mean ± SD as determined by triple assays. $^{**}p < 0.01$, $^{***}p < 0.001$, and $^{****}p < 0.0001$ by one-way ANOVA, followed by Dunnett's multiple comparisons test.

the mice injected with DIO3OS-silenced A549 cells exhibited more lung tumorigenesis and metastases compared to those injected with control A549 cells (Figure 5E). Histological analysis of lungs revealed that DIO3OS-silenced A549 cells formed a greater number of lung metastatic nodules and larger nodular diameter compared to control A549 cells (Figures 5F–5H). Taken together, these findings demonstrated that DIO3OS repressed NSCLC tumorigenesis and metastasis *in vivo*, which also supports the tumor-suppressive roles of DIO3OS in NSCLC.

DIO3OS competitively binds to heterogeneous nuclear ribonucleoprotein K (hnRNPK) and abrogates the effects of hnRNPK on MYC transcription and translation

One of the most common functional mechanisms of lncRNAs is to bind proteins.[40,41] To investigate this potential mechanism for DIO3OS, we utilized the online tool A database of RNA-binding proteins and associated motifs (ATtRACT) (https://attract.cnic.es/) to predict the proteins potentially interacting with DIO3OS. This analysis predicted hnRNPK as a potential

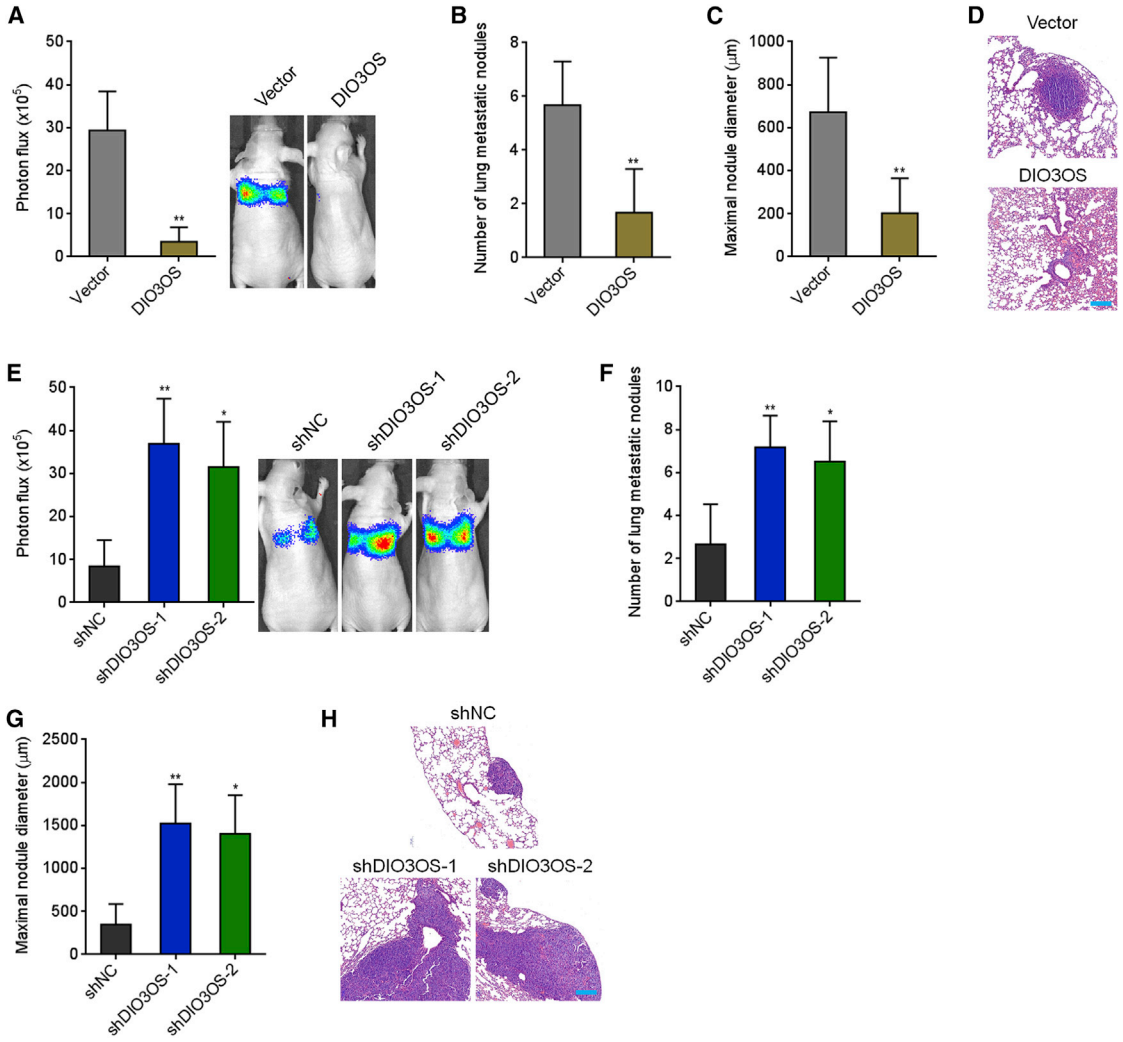

Figure 5. DIO3OS repressed NSCLC tumorigenesis and metastasis *in vivo*

(A–D) Luciferase-labeled H1299 cells with DIO3OS stable overexpression or control were injected into tail vein of nude mice. Bioluminescence analyses of lung metastasis at day 49 and the representative images of mice are shown in (A). Lung metastatic nodule numbers at day 49 are shown in (B). Maximal nodule diameters are shown in (C). Representative images of lung H&E staining are shown in (D). Scale bars, 200 μm. (E–H) Luciferase-labeled A549 cells with DIO3OS stable knockdown or control were injected into tail vein of nude mice. Bioluminescence analyses of lung metastasis at day 49 and the representative images of mice are shown in (E). Lung metastatic nodule numbers at day 49 are shown in (F). Maximal nodule diameters are shown in (G). Representative images of lung H&E staining are shown in (H). Scale bars, 200 μm. Data are shown as mean ± SD, as determined by n = 6 mice in each group. *$p < 0.05$ and **$p < 0.01$ by Mann Whitney test (A–C) or Kruskal-Wallis test, followed by Dunn's multiple comparisons test (E–G).

DIO3OS-interacting protein (Table S2). The predicted binding motif was located on the 398–420 nt of DIO3OS (CCUACCC CUCCCCAACUCAAUCC). The recently reported hnRNPK binding motif CCUCCCC was also located in this region.[42] Another online tool RNA-Protein Interaction Prediction (RPISeq) (http://pridb.gdcb.iastate.edu/RPISeq/) predicted the hnRNPK-DIO3OS interaction probability score of 0.9 (probability score >0.5 was considered positive). The third online tool RBPmap (http://rbpmap.technion.ac.il/) also predicted hnRNPK binding motif in this region (Table S3). Therefore, we focused on hnRNPK. RNA pull-down assays followed by western blot analyses using sense or antisense strand of biotin-labeled DIO3OS revealed the specific enrichment of hnRNPK in sense strand of DIO3OS group (Figure 6A). Additionally, biotinylated oligonucleotide probes complementary to DIO3OS were utilized to enrich DIO3OS and its interacted proteins. The results revealed that DIO3OS was successfully enriched by DIO3OS probes and also hnRNPK was specifically enriched by DIO3OS probes (Figure 6B). In a reciprocal experiment, RNA immunoprecipitation (RIP) assays using hnRNPK-specific antibodies showed the specific enrichment of DIO3OS in hnRNPK antibody group (Figure 6C). These data supported the interaction between DIO3OS and hnRNPK.

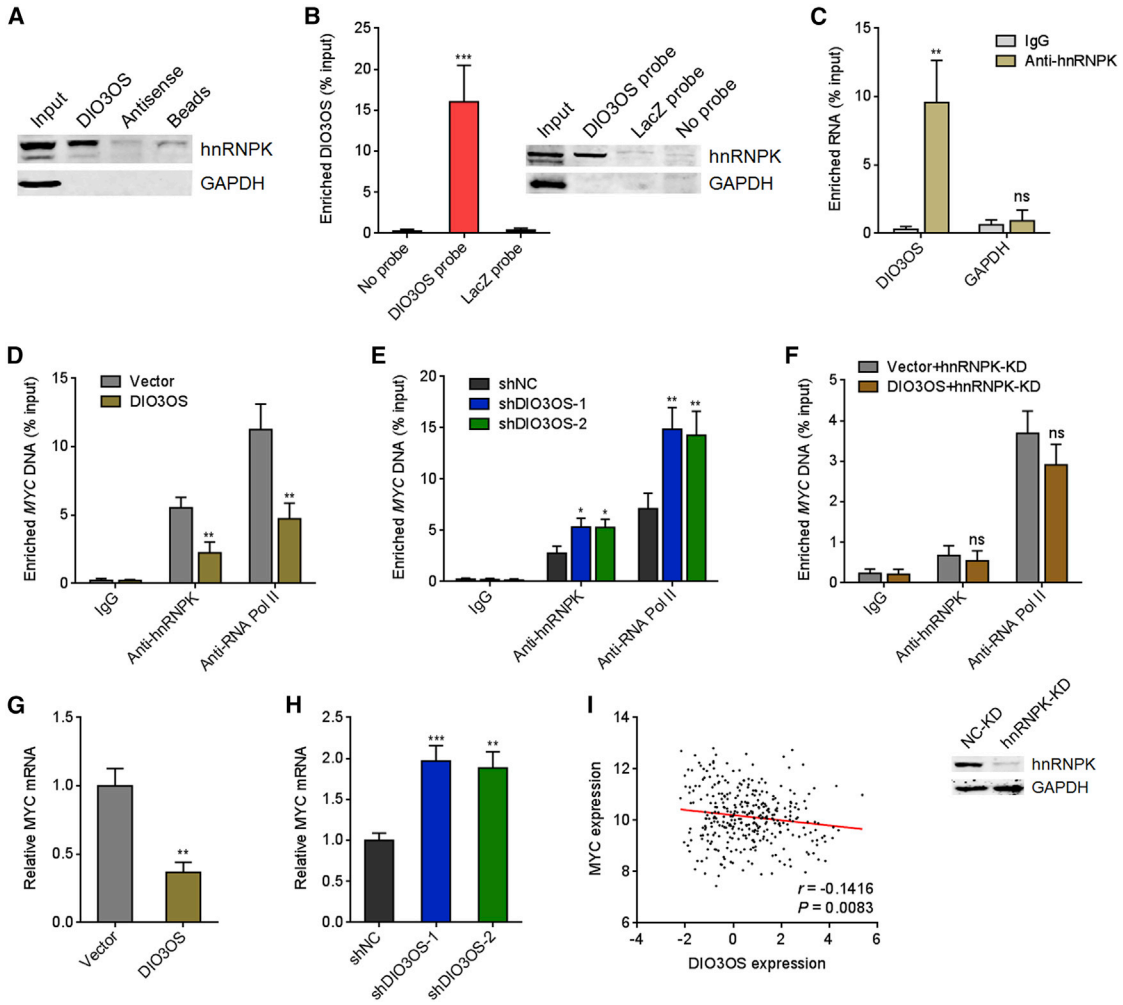

Figure 6. DIO3OS bound to hnRNPK and repressed the promoting effects of hnRNPK on *MYC* transcription

(A) RNA pull-down assays using biotin-labeled sense or antisense strand of DIO3OS, followed by western blot to detect the binding of hnRNPK or GAPDH protein to DIO3OS. (B) Biotinylated oligonucleotide probes complementary to DIO3OS were utilized to enrich DIO3OS and its interacted proteins. The enrichment of DIO3OS was detected by quantitative real-time PCR. The enrichment of hnRNPK or GAPDH protein was detected by western blot. (C) RIP assays using hnRNPK-specific antibody were conducted in A549 cells, followed by quantitative real-time PCR to detect the binding of DIO3OS or GAPDH mRNA to hnRNPK. (D) ChIP assays using hnRNPK- or RNA-Pol-II-specific antibodies were conducted in H1299 cells with DIO3OS overexpression or control, followed by quantitative real-time PCR to detect the binding of hnRNPK and RNA Pol II to *MYC* DNA. (E) ChIP assays using hnRNPK- or RNA-Pol-II-specific antibodies were conducted in A549 cells with DIO3OS knockdown or control, followed by quantitative real-time PCR to detect the binding of hnRNPK and RNA Pol II to *MYC* DNA. (F) ChIP assays using hnRNPK- or RNA-Pol-II-specific antibodies were conducted in H1299 cells with DIO3OS overexpression or control and concurrent hnRNPK depletion, followed by quantitative real-time PCR to detect the binding of hnRNPK and RNA Pol II to *MYC* DNA. (G) MYC expressions in H1299 cells with DIO3OS overexpression or control were measured by quantitative real-time PCR. (H) MYC expressions in A549 cells with DIO3OS knockdown or control were measured by quantitative real-time PCR. (I) The correlation between MYC expression and DIO3OS expression from TCGA LUAD dataset is shown. Data are shown as mean ± SD, as determined by triple assays.*p < 0.05, **p < 0.01, ***p < 0.001, and ns, not significant, by Student's t test (C, D, F, and G) or one-way ANOVA followed by Dunnett's multiple comparisons test (B, E, and H).

hnRNPK is a pivotal nucleic acid binding protein.[43] Several reports have revealed the oncogenic roles of hnRNPK in lung cancer.[44,45] Furthermore, classical oncogene *MYC* was identified as an important target of hnRNPK.[42,46] hnRNPK is necessary for the binding of RNA polymerase II (RNA Pol II) to *MYC* and therefore promotes *MYC* transcription.[46] To reveal whether DIO3OS modulates the effects of hnRNPK on *MYC*, we first detected the binding of hnRNPK and RNA Pol II to *MYC* after DIO3OS overexpression or depletion using chromatin immunoprecipitation (ChIP) assays. The results revealed that the binding of hnRNPK and RNA Pol II to *MYC* was remarkably repressed after DIO3OS overexpression and increased after DIO3OS depletion (Figures 6D and 6E). hnRNPK knockdown abrogated the effects of DIO3OS on the binding of hnRNPK and RNA Pol II to *MYC* (Figure 6F). Next, the effects of DIO3OS on *MYC* transcription were detected. As expected, MYC mRNA levels were downregulated after DIO3OS overexpression and upregulated

after DIO3OS depletion (Figures 6G and 6H). MYC expression was inversely correlated with DIO3OS expression in LUAD from TCGA dataset (Figure 6I), supporting the negative regulation of *MYC* transcription by DIO3OS.

Apart from the activation of *MYC* transcription, hnRNPK was also revealed to bind MYC mRNA 5′ UTR and promote MYC mRNA translation.[47,48] Thus, we further investigated the potential influences of DIO3OS on MYC translation. RIP assays revealed that the binding of hnRNPK to MYC mRNA was significantly reduced after DIO3OS overexpression and increased after DIO3OS depletion (Figures 7A and 7B). MYC 5′ UTR was inserted into upstream of firefly luciferase encoding gene. Dual-luciferase reporter assays revealed that luciferase activities of the constructed reporter containing MYC 5′ UTR were downregulated after DIO3OS overexpression and increased after DIO3OS depletion (Figures 7C and 7D). The influences of DIO3OS on MYC 5′ UTR luciferase activities were abrogated by hnRNPK knockdown (Figure 7E). MYC protein levels were remarkably downregulated after DIO3OS overexpression and significantly upregulated after DIO3OS depletion (Figures 7F and 7G). Taken together, these data suggested that DIO3OS not only repressed *MYC* transcription but also repressed MYC translation through competitively binding hnRNPK.

CDC25A is an important MYC downstream target.[49] TCGA LUAD dataset also showed the positive correlation between MYC expression and CDC25A expression (Figure 7H). Thus, to further validate the effects of DIO3OS on MYC, CDC25A expressions after DIO3OS overexpression or depletion were detected. The results revealed that CDC25A mRNA levels were remarkably downregulated after DIO3OS overexpression and remarkably upregulated after DIO3OS depletion (Figures 7I and 7J). CDC25A expression was inversely correlated with DIO3OS expression in LUAD from TCGA dataset (Figure 7K), further supporting the negative regulation of CDC25A by DIO3OS. Consistently, CDC25A protein levels were remarkably downregulated after DIO3OS overexpression and upregulated after DIO3OS depletion (Figures 7L and 7M). These data demonstrated that DIO3OS competitively bound hnRNPK and abrogated the positive effects of hnRNPK on MYC transcription and translation, resulting in the repression of MYC-CDC25A expression.

hnRNPK is required for the tumor-suppressive roles of DIO3OS in NSCLC

To elucidate whether hnRNPK is the critical mediator of the tumor-suppressive roles of DIO3OS in NSCLC, we detected the biological roles of DIO3OS in NSCLC at the absence of hnRNPK. CCK-8 assays revealed that hnRNPK absence abolished the reduced H1299 cell growth caused by DIO3OS overexpression (Figure 8A, compared to Figure 3C). Consistently, EdU incorporation assays revealed that hnRNPK absence abolished the reduced EdU-positive cell number caused by DIO3OS overexpression (Figure 8B, compared to Figure 3E). These results suggested that the repressive roles of DIO3OS on NSCLC cell growth were dependent on hnRNPK. Caspase-3 activity assays revealed that hnRNPK absence abolished the increased caspase-3 activity caused by DIO3OS overexpression (Figure 8C, compared to Figure 3G), suggesting that the promoting roles of DIO3OS on NSCLC cell apoptosis were dependent on hnRNPK. Transwell migration assays revealed that hnRNPK absence abolished the reduced cell migration abilities of H1299 cells caused by DIO3OS overexpression (Figure 8D, compared to Figure 3I). Transwell invasion assays revealed that hnRNPK absence abolished the reduced cell invasion abilities of H1299 cells caused by DIO3OS overexpression (Figure 8E, compared to Figure 3K). These results suggested that the repressive roles of DIO3OS on NSCLC cell motility were also dependent on hnRNPK.

DISCUSSION

DIO3OS arises from the antisense strand of DIO3OS and is located in chromosome 14q32.31. Recent reports revealed the downregulation of DIO3OS in cervical cancer and hepatocellular carcinoma but the upregulation of DIO3OS in pancreatic cancer.[50–52] In this study, we first reported the downregulation of DIO3OS in NSCLC. Furthermore, we demonstrated that low expression of DIO3OS is correlated with NSCLC progression and poor prognosis. Functional experiments revealed the tumor-suppressive roles of DIO3OS. Thus, our study identified DIO3OS as a NSCLC-related lncRNA.

Through analyzing TCGA dataset, we found that DIO3OS is downregulated in both LUAD and LUSC. In our tissues, we found the DIO3OS is also downregulated in NSCLC, and its expression is not correlated with histologic types. Additionally, low expression of DIO3OS is found to be correlated with local invasion, lymphatic metastasis, and TNM stages. Kaplan-Meier survival analyses in multiple cohorts all demonstrated that low expression of DIO3OS is related to worse overall survival. Therefore, in this study, we identified DIO3OS as a downregulated and prognosis-correlated lncRNA in NSCLC. Our study provided a biomarker for NSCLC and also evidence to support the clinical significances of lncRNAs in NSCLC.

Several factors may modulate the expression of lncRNAs, such as transcription factors, histone acetylation, and histone methylation.[53–58] The oncogenic lncRNA KTN1-AS1 was upregulated by STAT1 in NSCLC.[53] lncRNA TUG1 was reported to be induced in p53 in NSCLC.[54] SNHG3 was activated by E2F1 in NSCLC.[55] AC020978 was transactivated by hypoxia-inducible factor-1α.[56] Histone H3K27 acetylation induced the upregulation of LINC00467.[57] Histone H3K9 demethylation upregulated MALAT1 expression.[58] In this study, we found that DNA methylation also contributes to the dysregulation of lncRNAs in NSCLC. The CpG island CpG456 methylation at *DIO3OS* promoter region repressed DIO3OS expression. Thus, we identified DIO3OS as a DNA-methylation-repressed lncRNA.

Gain- and loss-of-function assays revealed that DIO3OS repressed NSCLC cell growth and motility and promoted NSCLC cell apoptosis *in vitro*. DIO3OS was also revealed to repress NSCLC tumorigenesis and lung metastasis *in vivo*. Thus, our study demonstrated that

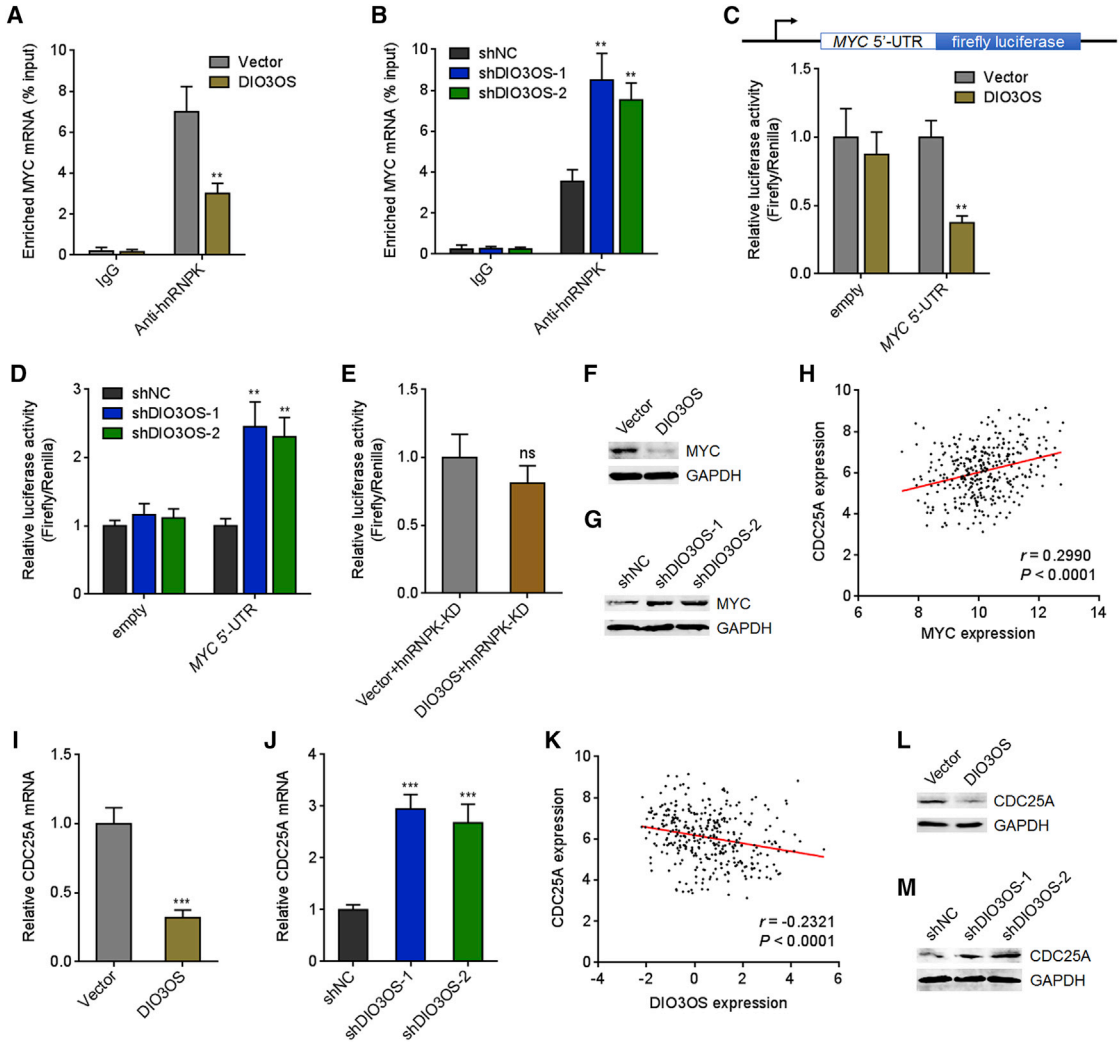

Figure 7. DIO3OS repressed the promoting effects of hnRNPK on MYC translation, resulting in downregulation of MYC and CDC25A

(A) RIP assays using hnRNPK-specific antibody were conducted in H1299 cells with DIO3OS overexpression or control, followed by quantitative real-time PCR to detect the binding of MYC mRNA to hnRNPK. (B) RIP assays using hnRNPK-specific antibody were conducted in A549 cells with DIO3OS knockdown or control, followed by quantitative real-time PCR to detect the binding of MYC mRNA to hnRNPK. (C) Schematic structure of the constructed MYC 5′ UTR firefly luciferase reporter is shown. After transient co-transfection of the constructed reporter and pRL-TK (encoding Renilla luciferase) into H1299 cells with DIO3OS overexpression or control, luciferase activities were measured by dual-luciferase reporter assays. Results are shown as relative ratio of firefly luciferase activity to Renilla luciferase activity. (D) After transient co-transfection of the constructed MYC 5′ UTR reporter and pRL-TK into A549 cells with DIO3OS knockdown or control, luciferase activities were measured by dual-luciferase reporter assays. Results are shown as relative ratio of firefly luciferase activity to Renilla luciferase activity. (E) After transient co-transfection of the constructed MYC 5′ UTR reporter and pRL-TK into H1299 cells with DIO3OS overexpression or control and concurrent hnRNPK depletion, luciferase activities were measured by dual-luciferase reporter assays. Results are shown as relative ratio of firefly luciferase activity to Renilla luciferase activity. (F) MYC protein levels in H1299 cells with DIO3OS overexpression or control were measured by western blot. (G) MYC protein levels in A549 cells with DIO3OS knockdown or control were measured by western blot. (H) The correlation between CDC25A expression and MYC expression from TCGA LUAD dataset is shown. (I) CDC25A expressions in H1299 cells with DIO3OS overexpression or control were measured by quantitative real-time PCR. (J) CDC25A expressions in A549 cells with DIO3OS knockdown or control were measured by quantitative real-time PCR. (K) The correlation between CDC25A expression and DIO3OS expression from TCGA LUAD dataset is shown. (L) CDC25A protein levels in H1299 cells with DIO3OS overexpression or control were measured by western blot. (M) CDC25A protein levels in A549 cells with DIO3OS knockdown or control were measured by western blot. Data are shown as mean ± SD, as determined by triple assays. **$p < 0.01$, ***$p < 0.001$, and ns by Student's t test (A, C, E, and I) or one-way ANOVA followed by Dunnett's multiple comparisons test (B, D, and J).

DIO3OS has tumor-suppressive roles in NSCLC and suggested that enhancing DIO3OS may be potential therapeutic strategy against NSCLC.

The combination of bioinformatic prediction and experimental verification identified hnRNPK as a critical interaction protein of DIO3OS. The expression and roles of hnRNPK in different cancers are

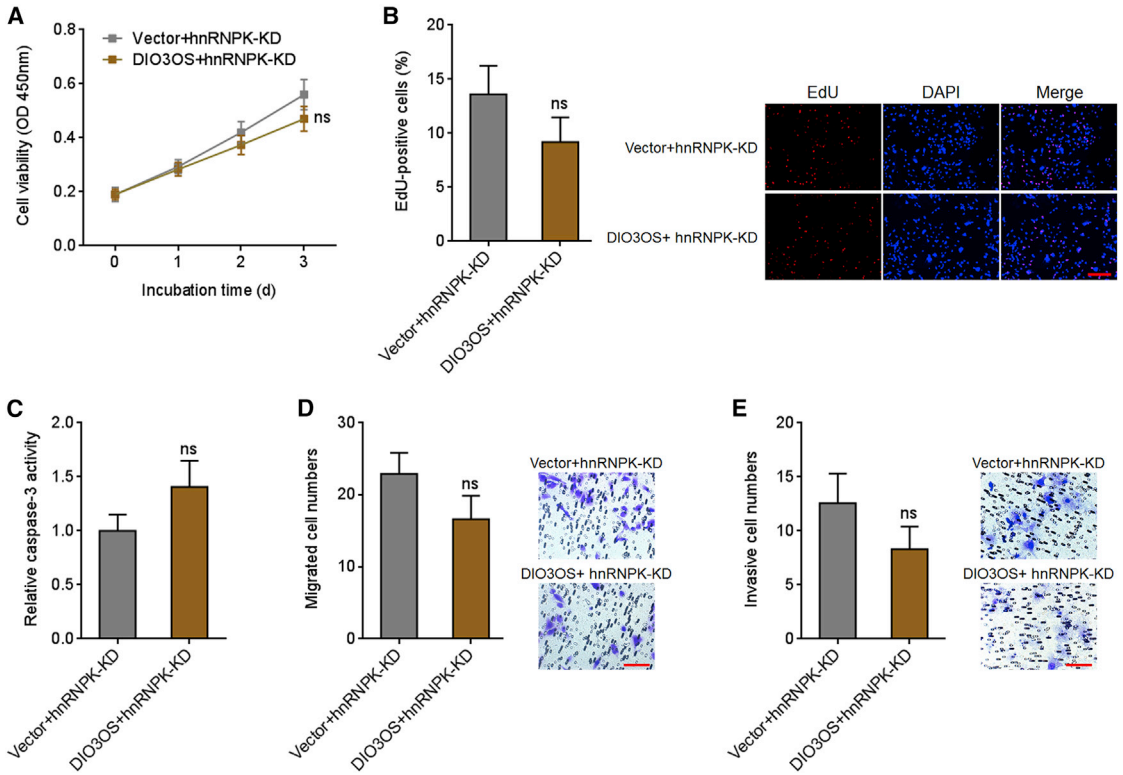

Figure 8. Absence of hnRNPK abrogated the repressive roles of DIO3OS on NSCLC cell growth and motility and the promoting roles of DIO3OS on NSCLC cell apoptosis

(A) Cell growth of H1299 cells with DIO3OS overexpression or control and concurrent hnRNPK depletion was measured by CCK-8 assays. (B) Cell growth of H1299 cells with DIO3OS overexpression or control and concurrent hnRNPK depletion was measured by EdU incorporation assays. Scale bars, 200 μm. (C) The activities of caspase-3 in cell lysates of H1299 cells with DIO3OS overexpression or control and concurrent hnRNPK depletion were measured to indicate cell apoptosis. (D) Cell migration of H1299 cells with DIO3OS overexpression or control and concurrent hnRNPK depletion was measured by transwell migration assays. Scale bars, 100 μm. (E) Cell invasion of H1299 cells with DIO3OS overexpression or control and concurrent hnRNPK depletion was measured by transwell invasion assays. Scale bars, 100 μm. Data are shown as mean ± SD as determined by triple assays. ns by Student's t test.

different.[43,59] In NSCLC, hnRNPK was reported to promote NSCLC growth and metastasis.[44,45] As a nucleic acid binding protein, hnRNPK exhibits a variety of complex mechanisms, such as regulating transcription, pre-mRNA splicing, mRNA metabolism, and mRNA translation.[42,47] *MYC* is a well-known oncogene in many cancers, including NSCLC.[60,61] Additionally, MYC is also revealed to be a critical downstream target of hnRNPK.[42,46,47] hnRNPK was necessary for RNA Pol II to bind *MYC* and promote *MYC* transcription.[46] Furthermore, hnRNPK was also revealed to promote MYC translation via binding MYC mRNA 5′ UTR.[47,48] In this study, we found that DIO3OS competitively bound to hnRNPK and repressed the binding of hnRNPK and RNA Pol II to *MYC* DNA, leading to the repression of *MYC* transcription. Furthermore, through competitively binding hnRNPK, DIO3OS also repressed the binding of hnRNPK to MYC mRNA, leading to the repression of MYC mRNA translation. Therefore, DIO3OS remarkably repressed the expression of MYC. CDC25A was reported as a downstream target of MYC.[49] Consistently, through repressing MYC, DIO3OS also repressed CDC25A expression in NSCLC. The inverse correlation between the expression of DIO3OS and MYC, CDC25A supported the repressive roles of DIO3OS on MYC and CDC25A. Moreover, absence of hnRNPK abolished the tumor-suppressive roles of DIO3OS in NSCLC, suggesting hnRNPK as a critical functional mediator of DIO3OS.

In conclusion, our findings identified DIO3OS as a DNA-methylation-repressed and lowly expressed lncRNA in NSCLC, whose low expression is related with poor prognosis. DIO3OS exhibited tumor-suppressive roles in NSCLC through competitively binding hnRNPK, reducing the binding of hnRNPK to *MYC* DNA and MYC mRNA, reversing the promoting roles of hnRNPK on *MYC* transcription and translation, leading to the repression of *MYC* transcription and translation, and therefore significantly repressing MYC and CDC25A expression.

MATERIALS AND METHODS

Human tissue

Seventy-eight pairs of NSCLC tissues and matched adjacent normal lung tissues were obtained from NSCLC patients who received

surgery resection at Guangzhou First People's Hospital. All tissues were examined by histopathological diagnosis and stored at −80°C until use. This study was conducted in accordance with the standards set by the Declaration of Helsinki and approved by the Review Board of Guangzhou First People's Hospital.

Cell culture and treatment

Human NSCLC cell lines H1299, H1975, and A549 were acquired from the American Type Culture Collection (ATCC) (Manassas, VA, USA). H1299 and H1975 cells were cultured in RPMI1640 Medium (Invitrogen, Carlsbad, CA, USA) added with 10% fetal bovine serum (FBS) (Invitrogen). A549 cells were cultured in F12K Medium (Invitrogen) added with 10% FBS. All cells were maintained in a humidified incubator containing 5% CO_2 at 37°C. Where indicated, A549 and H1299 cells were treated with 2.5 μM or 5 μM 5-Aza (Sigma-Aldrich, Merck KGaA, Darmstadt, Germany) for 3 days.

RNA extraction and quantitative real-time PCR

RNA extraction and quantitative real-time PCR were conducted as we previously described.[41] Briefly, total RNA was extracted from indicated tissues or cultured cells using TRIzol Regent (Invitrogen), followed by reverse transcription using the M-MLV Reverse Transcriptase (Invitrogen). Quantitative real-time PCR was conducted using the TB Green Premix Ex Taq (Takara, Kusatsu, Shiga, Japan) on ABI StepOnePlus Real-Time PCR System (Applied Biosystems, Foster City, CA, USA). The primers sequences were as follows: for DIO3OS, 5′-CCCGAACTGAGCCACCTT-3′ (forward) and 5′-CATTCACAGCCCCTGACG-3′ (reverse), NCBI Reference Sequence NR_152588.1, amplifying the 99–241 bp of DIO3OS with product length of 143 bp and annealing temperature 60°C; for MYC, 5′-TCTTCCCCTACCCTCTCAAC-3′ (forward) and 5′-CGATTTCTTCCTCATCTTCTTG-3′ (reverse), NCBI Reference Sequence NM_002467.6, amplifying the 989–1,195 bp of MYC with product length of 207 bp and annealing temperature 60°C; for CDC25A, 5′-TGGAGGTGAAGAACAACAGT-3′ (forward) and 5′-GGTCAAGAGAATCAGAATGG-3′ (reverse), NCBI Reference Sequence NM_001789.3, amplifying the 658–855 bp of CDC25A with product length of 198 bp and annealing temperature 56°C; and for GAPDH, 5′-GTCGGAGTCAACGGATTTG-3′ (forward) and 5′-TGGGTGGAATCATATTGGAA-3′ (reverse), NCBI Reference Sequence NM_002046.7, amplifying the 92–234 bp of GAPDH with product length of 143 bp and annealing temperature 60°C. GAPDH served as an endogenous control. The quantification of RNA expression was calculated using the comparative Ct method.

Vectors construction, siRNA, and transfection

To construct DIO3OS overexpression and *in vitro* transcription vector, DIO3OS full-length sequences were PCR amplified using the Phusion Flash High-Fidelity PCR Master Mix (Thermo Scientific, Rockford, IL, USA) with the primers 5′-CGGGATCCGCTTGCCTCGCCCAGC-3′ (forward) and 5′-GGAATTCAACGAGCACTCATTGTTTCGTGTTT-3′ (reverse). Next, the PCR products were inserted into the BamH I and EcoR I sites of the pcDNA3.1 vector (Invitrogen) to produce DIO3OS overexpression vector pcDNA3.1-DIO3OS. Additionally, the PCR products were also inserted into the BamH I and EcoR I sites of the pSPT19 vector (Roche, Mannheim, Germany) to produce DIO3OS *in vitro* transcription vector pSPT19-DIO3OS. To construct MYC 5′ UTR luciferase reporter, MYC 5′ UTR sequences were PCR amplified using the Phusion Flash High-Fidelity PCR Master Mix (Thermo Scientific) with the primers 5′-TGGTTTAGTGAACCGTGGATCCTGTAGTAATTCCAGCGAGAG-3′ (forward) and 5′-GGCGTCTTCCATGGTGGATCCAAGGAGAGCCTTTCAGAGA-3′ (reverse). Next, the PCR products were inserted into the BamH I site of the pMIR-REPORT vector (Applied Biosystems) using the NovoRec plus One step PCR Cloning Kit (Novoprotein, Shanghai, China) to produce MYC 5′ UTR luciferase reporter pMIR-REPORT-MYC-5′-UTR. ON-TARGETplus Human HNRNPK small interfering RNA (siRNA) reagents were obtained from Dharmacon (Cambridge, UK). The transfection of vectors and siRNAs was conducted using Lipofectamine 3000 (Invitrogen) according to the manufacturer's manual.

Stable cell lines construction

To construct NSCLC cells with DIO3OS stable overexpression, DIO3OS overexpression vector pcDNA3.1-DIO3OS was transfected into H1299 and H1975 cells. 72 h after transfection, the cells were selected with neomycin (500 μg/mL) for 4 weeks. To construct NSCLC cells with DIO3OS stable knockdown, two pairs of cDNA oligonucleotides against DIO3OS were synthesized and inserted into the shRNA lentivirus-expressing vector pLV3/H1/GFP&Puro (GenePharma, Shanghai, China), which was further used to produce shRNA lentiviruses targeting DIO3OS by GenePharma. Scrambled shRNA lentiviruses were used as negative control. The shRNA sequences were as follows: for shDIO3OS-1, 5′-GATCCGCCTCTGGATTTGGACCAACTTTCAAGAGAAGTTGGTCCAAATCCAGAGGCTTTTTTG-3′ (forward) and 5′-AATTCAAAAAAGCCTCTGGATTTGGACCAACTTCTCTTGAAAGTTGGTCCAAATCCAGAGGCG-3′ (reverse); for shDIO3OS-2, 5′-GATCCGCAGTAGCACTTGTAGCTATGTTCAAGAGACATAGCTACAAGTGCTACTGCTTTTTTG-3′ (forward) and 5′-AATTCAAAAAAGCAGTAGCACTTGTAGCTATGTCTCTTGAACATAGCTACAAGTGCTACTGCG-3′ (reverse); and for negative control (NC), 5′-GATCCGTTCTCCGAACGTGTCACGTTTCAAGAGAACGTGACACGTTCGGAGAACTTTTTTG-3′ (forward) and 5′-AATTCAAAAAAGTTCTCCGAACGTGTCACGTTCTCTTGAAACGTGACACGTTCGGAGAACG-3′ (reverse). Next, the shRNA lentiviruses targeting DIO3OS were infected into A549 cells. 96 h after transfection, the cells were selected with puromycin (1 μg/mL) for 4 weeks.

Cell growth and apoptosis assays

Cell growth ability was evaluated by CCK-8 and EdU incorporation assays. For CCK-8 assays, 2,000 indicated NSCLC cells were plated per well of 96-well plates. At indicated time points, 10 μL CCK-8 solution (Dojindo, Kumamoto, Japan) was added into the wells. After incubation for another 2 h, the absorbance at 450 nm was measured to indicate cell growth. EdU incorporation assay was conducted as we previously described using the EdU Kit (RiboBio, Guangzhou, China).[41] Results were quantified through counting at least ten

random fields. Cell apoptosis was evaluated through detecting the activity of caspase-3 in cell lysates using Caspase-3 Activity Assay Kit (Cell Signaling Technology, Boston, MA, USA).

Cell migration and invasion assays

Cell motility ability was evaluated using transwell migration and invasion assays as previously described.[62] Briefly, indicated NSCLC cells resuspended in serum-free medium were seeded into the top chambers of 24-well transwell inserts (BD Biosciences, San Jose, CA, USA) with (invasion) or without (migration) pre-coated Matrigel (BD Biosciences). Complete medium added with 10% FBS was placed into the lower chambers. After incubation for 48 h, cells remaining on the top chambers were wiped off while the cells that had traversed the membranes were fixed, stained, and counted based on at least ten random fields.

Mouse xenograft assays

Indicated luciferase-labeled NSCLC cells were injected into the tail veins of 5-week-old BALB/c nude mice. 49 days post-injection, the mice were intraperitoneally injected with 4.0 mg of luciferin (Caliper Life Sciences, Hopkinton, MA, USA) in 50 μL of saline. Then, 10 min later, the lung metastases were monitored by the IVIS@ Lumina II system (Caliper Life Sciences). The mice were sacrificed, and the lungs were resected and detected by hematoxylin and eosin (H&E) staining. The animal experiments were approved by the Review Board of Guangzhou First People's Hospital.

RNA pull-down assays

To detect the binding of proteins to DIO3OS, sense or antisense strands of biotin-labeled DIO3OS were *in vitro* transcribed from pSPT19-DIO3OS using the Biotin RNA Labeling Mix (Roche) and T7 or Sp6 RNA polymerase (Roche), respectively. After removal of DNA and purification using RNeasy Mini Kit (QIAGEN, Hilden, Germany), 3 μg of biotin-labeled sense or antisense strands of DIO3OS were incubated with 1 mg of whole-cell lysate of A549 cells for 1 h at 25°C. Next, the complexes were enriched by the streptavidin agarose beads (Invitrogen). The protein present in the enrichment was detected by western blot. Furthermore, the proteins bound to DIO3OS were also enriched using biotinylated oligonucleotide probes complementary to DIO3OS. The probes sequences were as follows: (1) 5′-AACGTCCGGGGACGAACG-3′; (2) 5′-AGGACACTTGACGCGTCC-3′; (3) 5′-CTACAAGTGCTACTGCAT-3′; (4) 5′-CTGCAGCTGGACAACGAA-3′; (5) 5′-TTGGGGAGGGGTAGGTAT-3′; (6) 5′-TGAGCTGGCCTGGCAGAC-3′; (7) 5′-TCTGAGATGTGCCAGCAC-3′; and (8) 5′-CGTGTTTATTTGTTACCC-3′. The enrichment of DIO3OS and DIO3OS-interacted proteins was conducted using the Magna ChIRP RNA Interactome Kits (Millipore, Bedford, MA, USA) and detected by quantitative real-time PCR and western blot, respectively.

RIP assay

To detect the binding of RNAs to hnRNPK, RIP assays were conducted in A549 cells using the Magna RIP RNA-Binding Protein Immunoprecipitation Kit (Millipore) and hnRNPK-specific antibody (Abcam, Cambridge, UK) according to the manufacturer's manual. The enrichment of RNAs was detected by quantitative real-time PCR.

ChIP assay

To detect the binding of hnRNPK and RNA Pol II to genomic DNA, ChIP assays were conducted in indicated NSCLC cells using the EZ-Magna ChIP A/G Chromatin Immunoprecipitation Kit (Millipore) and primary antibodies against hnRNPK (Abcam) or RNA Pol II (Millipore) according to the manufacturer's manuals. The enriched DNA was detected by quantitative real-time PCR with the primers for *MYC* genomic DNA 5′-CAAAAATGAGGGGCTGTGTT-3′ (forward) and 5′-GGCAAGGATTTGCTTTTCAG-3′ (reverse).[46]

Western blot

Western blot was conducted as we previously described.[41] Briefly, total proteins were extracted from indicated NSCLC cells using RIPA lysis buffer (Beyotime, Shanghai, China). Proteins enriched from RNA pull-down assays or extracted from cells (30 μg) were separated by sodium dodecyl sulfate polyacrylamide gel electrophoresis (SDS-PAGE), followed by being transferred into nitrocellulose membrane (Millipore). After blocking using 5% non-fat milk, the membranes were incubated with primary antibodies against hnRNPK (Abcam), GAPDH (Abcam), MYC (Cell Signaling Technology), or CDC25A (Cell Signaling Technology). The membranes were further incubated with horseradish peroxidase conjugated goat anti-rabbit or goat anti-mouse second antibodies, followed by visualization using enhanced chemiluminescence.

Dual-luciferase reporter assay

MYC 5′ UTR luciferase reporter pMIR-REPORT-MYC-5′-UTR or empty luciferase reporter pMIR-REPORT was co-transfected with pRL-TK vector (Promega, Madison, WI, USA) into indicated NSCLC cells. pRL-TK expressed Renilla luciferase and was used to monitor transfection efficiency. 48 h after transfection, the firefly luciferase activities and Renilla luciferase activities were measured using the Dual-Luciferase Reporter Assay System (Promega).

Bioinformatics analysis

The expressions of DIO3OS in NSCLC from TCGA dataset were analyzed by the online *in silico* tool Gene Expression Profiling Interactive Analysis (GEPIA) (http://gepia.cancer-pku.cn/). The correlation between DIO3OS expression and overall survival in NSCLC from TCGA dataset was analyzed by the online *in silico* tool R2 (https://hgserver1.amc.nl/cgi-bin/r2/main.cgi). The correlation between DIO3OS expression and overall survival in NSCLC was also analyzed in another dataset using the online *in silico* tool Kaplan-Meier Plotter (http://kmplot.com/analysis/). Methylation data of 17 methylation probes located on CpG456 were retrieved from TCGA Illumina Infinium Human DNA Methylation 450k BeadChip data using the online tool UCSC Xena (https://xenabrowser.net/heatmap/#). The bindings between lncRNAs and proteins were predicted using three online *in silico* tools: a database of RNA-binding proteins and associated motifs (ATtRACT) (https://attract.cnic.es/); RNA-Protein Interaction Prediction (RPISeq) (http://pridb.gdcb.iastate.edu/RPISeq/); and RBPmap (http://rbpmap.technion.ac.il/).

Statistical analysis

All statistical analyses were conducted using the GraphPad Prism 6.0 (GraphPad Software, La Jolla, CA). Comparisons between two groups were subjected to Wilcoxon matched-pairs signed rank test, Student's t test, or Mann Whitney test as indicated in figure legends. Comparisons between more than two groups were subjected to one-way ANOVA followed by Dunnett's multiple comparisons test or Kruskal-Wallis test followed by Dunn's multiple comparisons test as indicated in figure legends. Correlations between genes' expression and methylation probes were subjected to Pearson correlation analysis. $p < 0.05$ was considered as statistically significant.

SUPPLEMENTAL INFORMATION

Supplemental information can be found online at https://doi.org/10.1016/j.omto.2021.09.006.

ACKNOWLEDGMENTS

The study was supported by Guangzhou First People's Hospital.

AUTHOR CONTRIBUTIONS

M.Z. conceived and designed the study. Z.Z. and W.Z. advised on the experimental design. M.Z., J.W., and W.H. carried out the experiments. M.Z. and J.W. drafted the manuscript. All authors participated in the analysis and interpretation of data. All authors read and approved the final manuscript.

DECLARATION OF INTERESTS

The authors declare no competing interests.

REFERENCES

1. Liang, W., Liu, J., and He, J. (2020). Driving the improvement of lung cancer prognosis. Cancer Cell *38*, 449–451.
2. Sung, H., Ferlay, J., Siegel, R.L., Laversanne, M., Soerjomataram, I., Jemal, A., and Bray, F. (2021). Global cancer statistics 2020: GLOBOCAN estimates of incidence and mortality worldwide for 36 cancers in 185 countries. CA Cancer J. Clin. *71*, 209–249.
3. The, L.; The Lancet (2019). Lung cancer: some progress, but still a lot more to do. Lancet *394*, 1880.
4. Morris, L.G.T., and Chan, T.A. (2019). Lung cancer evolution: what's immunity got to do with it? Cancer Cell *35*, 711–713.
5. Alam, H., Tang, M., Maitituoheti, M., Dhar, S.S., Kumar, M., Han, C.Y., Ambati, C.R., Amin, S.B., Gu, B., Chen, T.Y., et al. (2020). KMT2D deficiency impairs super-enhancers to confer a glycolytic vulnerability in lung cancer. Cancer Cell *37*, 599–617.e7.
6. LaFave, L.M., Kartha, V.K., Ma, S., Meli, K., Del Priore, I., Lareau, C., Naranjo, S., Westcott, P.M.K., Duarte, F.M., Sankar, V., et al. (2020). Epigenomic state transitions characterize tumor progression in mouse lung adenocarcinoma. Cancer Cell *38*, 212–228.e13.
7. Guerra, S.L., Maertens, O., Kuzmickas, R., De Raedt, T., Adeyemi, R.O., Guild, C.J., Guillemette, S., Redig, A.J., Chambers, E.S., Xu, M., et al. (2020). A deregulated HOX gene axis confers an epigenetic vulnerability in KRAS-mutant lung cancers. Cancer Cell *37*, 705–719.e6.
8. Kong, X., Chen, J., Xie, W., Brown, S.M., Cai, Y., Wu, K., Fan, D., Nie, Y., Yegnasubramanian, S., Tiedemann, R.L., et al. (2019). Defining UHRF1 domains that support maintenance of human colon cancer DNA methylation and oncogenic properties. Cancer Cell *35*, 633–648.e7.
9. Yang, M., Wang, A., Li, C., Sun, J., Yi, G., Cheng, H., Liu, X., Wang, Z., Zhou, Y., Yao, G., et al. (2020). Methylation-induced silencing of ALDH2 facilitates lung adenocarcinoma bone metastasis by activating the MAPK pathway. Front. Oncol. *10*, 1141.
10. Wu, T.H., Chang, S.Y., Shih, Y.L., Chian, C.F., Chang, H., and Lin, Y.W. (2020). Epigenetic silencing of LMX1A contributes to cancer progression in lung cancer cells. Int. J. Mol. Sci. *21*, 5425.
11. Li, J., Li, M.H., Wang, T.T., Liu, X.N., Zhu, X.T., Dai, Y.Z., Zhai, K.C., Liu, Y.D., Lin, J.L., Ge, R.L., et al. (2021). SLC38A4 functions as a tumour suppressor in hepatocellular carcinoma through modulating Wnt/β-catenin/MYC/HMGCS2 axis. Br. J. Cancer *125*, 865–876.
12. Liang, G., Meng, W., Huang, X., Zhu, W., Yin, C., Wang, C., Fassan, M., Yu, Y., Kudo, M., Xiao, S., et al. (2020). miR-196b-5p-mediated downregulation of TSPAN12 and GATA6 promotes tumor progression in non-small cell lung cancer. Proc. Natl. Acad. Sci. USA *117*, 4347–4357.
13. Lu, J., Tan, T., Zhu, L., Dong, H., and Xian, R. (2020). Hypomethylation causes *MIR21* overexpression in tumors. Mol. Ther. Oncolytics *18*, 47–57.
14. Yuan, J.H., Yang, F., Chen, B.F., Lu, Z., Huo, X.S., Zhou, W.P., Wang, F., and Sun, S.H. (2011). The histone deacetylase 4/SP1/microrna-200a regulatory network contributes to aberrant histone acetylation in hepatocellular carcinoma. Hepatology *54*, 2025–2035.
15. Shi, D., Zhang, K., Li, G., and Zhao, Y. (2020). MiR-1471 protects the aggravation of non-small-cell lung carcinoma by targeting FOXL1. Biofactors *46*, 734–742.
16. Liu, X., Liu, B., Li, R., Wang, F., Wang, N., Zhang, M., Bai, Y., Wu, J., Liu, L., Han, D., et al. (2020). miR-146a-5p plays an oncogenic role in NSCLC via suppression of TRAF6. Front. Cell Dev. Biol. *8*, 847.
17. Iyer, M.K., Niknafs, Y.S., Malik, R., Singhal, U., Sahu, A., Hosono, Y., Barrette, T.R., Prensner, J.R., Evans, J.R., Zhao, S., et al. (2015). The landscape of long noncoding RNAs in the human transcriptome. Nat. Genet. *47*, 199–208.
18. Ponting, C.P., Oliver, P.L., and Reik, W. (2009). Evolution and functions of long noncoding RNAs. Cell *136*, 629–641.
19. Hanniford, D., Ulloa-Morales, A., Karz, A., Berzoti-Coelho, M.G., Moubarak, R.S., Sánchez-Sendra, B., Kloetgen, A., Davalos, V., Imig, J., Wu, P., et al. (2020). Epigenetic silencing of CDR1as drives IGF2BP3-mediated melanoma invasion and metastasis. Cancer Cell *37*, 55–70.e15.
20. Yuan, J.H., Yang, F., Wang, F., Ma, J.Z., Guo, Y.J., Tao, Q.F., Liu, F., Pan, W., Wang, T.T., Zhou, C.C., et al. (2014). A long noncoding RNA activated by TGF-β promotes the invasion-metastasis cascade in hepatocellular carcinoma. Cancer Cell *25*, 666–681.
21. Mo, S., Zhang, L., Dai, W., Han, L., Wang, R., Xiang, W., Wang, Z., Li, Q., Yu, J., Yuan, J., et al. (2020). Antisense lncRNA LDLRAD4-AS1 promotes metastasis by decreasing the expression of LDLRAD4 and predicts a poor prognosis in colorectal cancer. Cell Death Dis. *11*, 155.
22. Wu, S., Nitschke, K., Worst, T.S., Fierek, A., Weis, C.A., Eckstein, M., Porubsky, S., Kriegmair, M., and Erben, P. (2020). Long noncoding RNA MIR31HG and its splice variants regulate proliferation and migration: prognostic implications for muscle invasive bladder cancer. J. Exp. Clin. Cancer Res. *39*, 288.
23. Saeinasab, M., Bahrami, A.R., González, J., Marchese, F.P., Martinez, D., Mowla, S.J., Matin, M.M., and Huarte, M. (2019). SNHG15 is a bifunctional MYC-regulated noncoding locus encoding a lncRNA that promotes cell proliferation, invasion and drug resistance in colorectal cancer by interacting with AIF. J. Exp. Clin. Cancer Res. *38*, 172.
24. Barbagallo, C., Brex, D., Caponnetto, A., Cirnigliaro, M., Scalia, M., Magnano, A., Caltabiano, R., Barbagallo, D., Biondi, A., Cappellani, A., et al. (2018). LncRNA UCA1, upregulated in CRC biopsies and downregulated in serum exosomes, controls mRNA expression by RNA-RNA interactions. Mol. Ther. Nucleic Acids *12*, 229–241.
25. Arshi, A., Sharifi, F.S., Khorramian Ghahfarokhi, M., Faghih, Z., Doosti, A., Ostovari, S., Mahmoudi Maymand, E., and Ghahramani Seno, M.M. (2018). Expression analysis of MALAT1, GAS5, SRA, and NEAT1 lncRNAs in breast cancer tissues from young women and women over 45 years of age. Mol. Ther. Nucleic Acids *12*, 751–757.
26. Luo, H., Zhu, G., Xu, J., Lai, Q., Yan, B., Guo, Y., Fung, T.K., Zeisig, B.B., Cui, Y., Zha, J., et al. (2019). HOTTIP lncRNA promotes hematopoietic stem cell self-renewal leading to AML-like disease in mice. Cancer Cell *36*, 645–659.e8.
27. Esposito, R., Bosch, N., Lanzós, A., Polidori, T., Pulido-Quetglas, C., and Johnson, R. (2019). Hacking the cancer genome: profiling therapeutically actionable long noncoding RNAs using CRISPR-Cas9 screening. Cancer Cell *35*, 545–557.

28. Zhang, Y., Li, Y., Hu, Q., Xi, Y., Xing, Z., Zhang, Z., Huang, L., Wu, J., Liang, K., Nguyen, T.K., et al. (2020). The lncRNA H19 alleviates muscular dystrophy by stabilizing dystrophin. Nat. Cell Biol. *22*, 1332–1345.

29. Daneshvar, K., Ardehali, M.B., Klein, I.A., Hsieh, F.K., Kratkiewicz, A.J., Mahpour, A., Cancelliere, S.O.L., Zhou, C., Cook, B.M., Li, W., et al. (2020). lncRNA DIGIT and BRD3 protein form phase-separated condensates to regulate endoderm differentiation. Nat. Cell Biol. *22*, 1211–1222.

30. Yuan, J.H., Liu, X.N., Wang, T.T., Pan, W., Tao, Q.F., Zhou, W.P., Wang, F., and Sun, S.H. (2017). The MBNL3 splicing factor promotes hepatocellular carcinoma by increasing PXN expression through the alternative splicing of lncRNA-PXN-AS1. Nat. Cell Biol. *19*, 820–832.

31. Zhu, X.T., Yuan, J.H., Zhu, T.T., Li, Y.Y., and Cheng, X.Y. (2016). Long noncoding RNA glypican 3 (GPC3) antisense transcript 1 promotes hepatocellular carcinoma progression via epigenetically activating GPC3. FEBS J. *283*, 3739–3754.

32. Dong, P., Xiong, Y., Yue, J., Xu, D., Ihira, K., Konno, Y., Kobayashi, N., Todo, Y., and Watari, H. (2019). Long noncoding RNA NEAT1 drives aggressive endometrial cancer progression via miR-361-regulated networks involving STAT3 and tumor microenvironment-related genes. J. Exp. Clin. Cancer Res. *38*, 295.

33. Sikora, M., Marycz, K., and Smieszek, A. (2020). Small and long non-coding RNAs as functional regulators of bone homeostasis, acting alone or cooperatively. Mol. Ther. Nucleic Acids *21*, 792–803.

34. Gao, W., Qi, C.Q., Feng, M.G., Yang, P., Liu, L., and Sun, S.H. (2020). SOX2-induced upregulation of lncRNA LINC01561 promotes non-small-cell lung carcinoma progression by sponging miR-760 to modulate SHCBP1 expression. J. Cell. Physiol. *235*, 6684–6696.

35. Huang, J., Pan, B., Xia, G., Zhu, J., Li, C., and Feng, J. (2020). LncRNA SNHG15 regulates EGFR-TKI acquired resistance in lung adenocarcinoma through sponging miR-451 to upregulate MDR-1. Cell Death Dis. *11*, 525.

36. Chen, J., Liu, A., Wang, Z., Wang, B., Chai, X., Lu, W., Cao, T., Li, R., Wu, M., Lu, Z., et al. (2020). LINC00173.v1 promotes angiogenesis and progression of lung squamous cell carcinoma by sponging miR-511-5p to regulate VEGFA expression. Mol. Cancer *19*, 98.

37. Chen, L., Li, X., Lu, C., Zhao, Y., Zhu, J., and Yang, L. (2020). The long non-coding RNA CASC7 inhibits growth and invasion of non-small cell lung cancer cells through phosphatase and tensin homolog upregulation via sequestration of miR-92a. Int. J. Oncol. *57*, 466–477.

38. Yang, W., Qian, Y., Gao, K., Zheng, W., Wu, G., He, Q., Chen, Q., Song, Y., Wang, L., Wang, Y., et al. (2021). LncRNA BRCAT54 inhibits the tumorigenesis of non-small cell lung cancer by binding to RPS9 to transcriptionally regulate JAK-STAT and calcium pathway genes. Carcinogenesis *42*, 80–92.

39. Tan, B.S., Yang, M.C., Singh, S., Chou, Y.C., Chen, H.Y., Wang, M.Y., Wang, Y.C., and Chen, R.H. (2019). LncRNA NORAD is repressed by the YAP pathway and suppresses lung and breast cancer metastasis by sequestering S100P. Oncogene *38*, 5612–5626.

40. Li, J.K., Chen, C., Liu, J.Y., Shi, J.Z., Liu, S.P., Liu, B., Wu, D.S., Fang, Z.Y., Bao, Y., Jiang, M.M., et al. (2017). Long noncoding RNA MRCCAT1 promotes metastasis of clear cell renal cell carcinoma via inhibiting NPR3 and activating p38-MAPK signaling. Mol. Cancer *16*, 111.

41. Zhang, M., Wu, J., Zhong, W., Zhao, Z., and Liu, Z. (2018). Long non-coding RNA BRE-AS1 represses non-small cell lung cancer cell growth and survival via up-regulating NR4A3. Arch. Biochem. Biophys. *660*, 53–63.

42. Cai, Z., Cao, C., Ji, L., Ye, R., Wang, D., Xia, C., Wang, S., Du, Z., Hu, N., Yu, X., et al. (2020). RIC-seq for global in situ profiling of RNA-RNA spatial interactions. Nature *582*, 432–437.

43. Wang, Z., Qiu, H., He, J., Liu, L., Xue, W., Fox, A., Tickner, J., and Xu, J. (2020). The emerging roles of hnRNPK. J. Cell. Physiol. *235*, 1995–2008.

44. Li, M., Zhang, W., Yang, X., Liu, H., Cao, L., Li, W., Wang, L., Zhang, G., and Gao, R. (2019). Downregulation of HNRNPK in human cancer cells inhibits lung metastasis. Animal Model. Exp. Med. *2*, 291–296.

45. Tang, F., Li, W., Chen, Y., Wang, D., Han, J., and Liu, D. (2014). Downregulation of hnRNP K by RNAi inhibits growth of human lung carcinoma cells. Oncol. Lett. *7*, 1073–1077.

46. Li, J., Chen, Y., Xu, X., Jones, J., Tiwari, M., Ling, J., Wang, Y., Harismendy, O., and Sen, G.L. (2019). HNRNPK maintains epidermal progenitor function through transcription of proliferation genes and degrading differentiation promoting mRNAs. Nat. Commun. *10*, 4198.

47. Evans, J.R., Mitchell, S.A., Spriggs, K.A., Ostrowski, J., Bomsztyk, K., Ostarek, D., and Willis, A.E. (2003). Members of the poly (rC) binding protein family stimulate the activity of the c-myc internal ribosome entry segment in vitro and in vivo. Oncogene *22*, 8012–8020.

48. Notari, M., Neviani, P., Santhanam, R., Blaser, B.W., Chang, J.S., Galietta, A., Willis, A.E., Roy, D.C., Caligiuri, M.A., Marcucci, G., and Perrotti, D. (2006). A MAPK/HNRPK pathway controls BCR/ABL oncogenic potential by regulating MYC mRNA translation. Blood *107*, 2507–2516.

49. Liu, H., Zhao, W.L., Wang, J.P., Xin, B.M., and Shao, R.G. (2018). EBP50 suppresses the proliferation of MCF-7 human breast cancer cells via promoting Beclin-1/p62-mediated lysosomal degradation of c-Myc. Acta Pharmacol. Sin. *39*, 1347–1358.

50. Roychowdhury, A., Samadder, S., Das, P., Mazumder, D.I., Chatterjee, A., Addya, S., Mondal, R., Roy, A., Roychoudhury, S., and Panda, C.K. (2020). Deregulation of H19 is associated with cervical carcinoma. Genomics *112*, 961–970.

51. Song, M., Zhong, A., Yang, J., He, J., Cheng, S., Zeng, J., Huang, Y., Pan, Q., Zhao, J., Zhou, Z., et al. (2019). Large-scale analyses identify a cluster of novel long noncoding RNAs as potential competitive endogenous RNAs in progression of hepatocellular carcinoma. Aging (Albany NY) *11*, 10422–10453.

52. Cui, K., Jin, S., Du, Y., Yu, J., Feng, H., Fan, Q., and Ma, W. (2019). Long noncoding RNA DIO3OS interacts with miR-122 to promote proliferation and invasion of pancreatic cancer cells through upregulating ALDOA. Cancer Cell Int. *19*, 202.

53. Liu, C., Li, X., Hao, Y., Wang, F., Cheng, Z., Geng, H., and Geng, D. (2020). STAT1-induced upregulation of lncRNA KTN1-AS1 predicts poor prognosis and facilitates non-small cell lung cancer progression via miR-23b/DEPDC1 axis. Aging (Albany NY) *12*, 8680–8701.

54. Zhang, E.B., Yin, D.D., Sun, M., Kong, R., Liu, X.H., You, L.H., Han, L., Xia, R., Wang, K.M., Yang, J.S., et al. (2014). P53-regulated long non-coding RNA TUG1 affects cell proliferation in human non-small cell lung cancer, partly through epigenetically regulating HOXB7 expression. Cell Death Dis. *5*, e1243.

55. Shi, J., Li, J., Yang, S., Hu, X., Chen, J., Feng, J., Shi, T., He, Y., Mei, Z., He, W., et al. (2020). LncRNA SNHG3 is activated by E2F1 and promotes proliferation and migration of non-small-cell lung cancer cells through activating TGF-β pathway and IL-6/JAK2/STAT3 pathway. J. Cell. Physiol. *235*, 2891–2900.

56. Hua, Q., Mi, B., Xu, F., Wen, J., Zhao, L., Liu, J., and Huang, G. (2020). Hypoxia-induced lncRNA-AC020978 promotes proliferation and glycolytic metabolism of non-small cell lung cancer by regulating PKM2/HIF-1α axis. Theranostics *10*, 4762–4778.

57. Zhu, Y., Li, J., Bo, H., He, D., Xiao, M., Xiang, L., Gong, L., Hu, Y., Zhang, Y., Cheng, Y., et al. (2020). LINC00467 is up-regulated by TDG-mediated acetylation in non-small cell lung cancer and promotes tumor progression. Oncogene *39*, 6071–6084.

58. Tee, A.E., Ling, D., Nelson, C., Atmadibrata, B., Dinger, M.E., Xu, N., Mizukami, T., Liu, P.Y., Liu, B., Cheung, B., et al. (2014). The histone demethylase JMJD1A induces cell migration and invasion by up-regulating the expression of the long noncoding RNA MALAT1. Oncotarget *5*, 1793–1804.

59. Qin, G., Tu, X., Li, H., Cao, P., Chen, X., Song, J., Han, H., Li, Y., Guo, B., Yang, L., et al. (2020). Long noncoding RNA p53-stabilizing and activating RNA promotes p53 signaling by inhibiting heterogeneous nuclear ribonucleoprotein K deSUMOylation and suppresses hepatocellular carcinoma. Hepatology *71*, 112–129.

60. Luanpitpong, S., Rodboon, N., Samart, P., Vinayanuwattikun, C., Klamkhlai, S., Chanvorachote, P., Rojanasakul, Y., and Issaragrisil, S. (2020). A novel TRPM7/O-GlcNAc axis mediates tumour cell motility and metastasis by stabilising c-Myc and caveolin-1 in lung carcinoma. Br. J. Cancer *123*, 1289–1301.

61. Sun, L., Wang, Y., Cen, J., Ma, X., Cui, L., Qiu, Z., Zhang, Z., Li, H., Yang, R.Z., Wang, C., et al. (2019). Modelling liver cancer initiation with organoids derived from directly reprogrammed human hepatocytes. Nat. Cell Biol. *21*, 1015–1026.

62. Liu, X.N., Yuan, J.H., Wang, T.T., Pan, W., and Sun, S.H. (2017). An alternative POLDIP3 transcript promotes hepatocellular carcinoma progression. Biomed. Pharmacother. *89*, 276–283.